

High-quality MgB₂ nanocrystals synthesized by using modified amorphous nano-boron powders: Study of defect structures and superconductivity properties

Cite as: AIP Advances 9, 045018 (2019); <https://doi.org/10.1063/1.5089488>

Submitted: 19 January 2019 . Accepted: 01 April 2019 . Published Online: 16 April 2019

Ali Bateni, Emre Erdem , Wolfgang Häßler , and Mehmet Somer



View Online



Export Citation



CrossMark

ARTICLES YOU MAY BE INTERESTED IN

[Effects of oxygen ion implantation on single-crystalline MgB₂ thin films](#)

Journal of Applied Physics **125**, 023904 (2019); <https://doi.org/10.1063/1.5061772>

[Enhancement of critical current density by borohydride pinning in H-doped MgB₂ bulks](#)

Journal of Applied Physics **125**, 113901 (2019); <https://doi.org/10.1063/1.5064498>

[Al-doped MgB₂ materials studied using electron paramagnetic resonance and Raman spectroscopy](#)

Applied Physics Letters **108**, 202601 (2016); <https://doi.org/10.1063/1.4949338>

AVS Quantum Science

Co-published with AIP Publishing



Coming Soon!

High-quality MgB₂ nanocrystals synthesized by using modified amorphous nano-boron powders: Study of defect structures and superconductivity properties

Cite as: AIP Advances 9, 045018 (2019); doi: 10.1063/1.5089488

Submitted: 19 January 2019 • Accepted: 1 April 2019 •

Published Online: 16 April 2019



View Online



Export Citation



CrossMark

Ali Bateni,^{1,2} Emre Erdem,^{3,4,a)}  Wolfgang Häßler,⁵  and Mehmet Somer^{1,a)}

AFFILIATIONS

¹Department of Chemistry, Koç University, Rumelifeneri Yolu, Sariyer, Istanbul, Turkey

²Duktus (Production) GmbH, Sophienstraße 52-54, Wetzlar, Germany

³Faculty of Engineering and Natural Sciences, Sabanci University, TR-34956 Istanbul, Turkey

⁴Sabanci University, SUNUM Nanotechnology Research Centre, TR-34956 Istanbul, Turkey

⁵Leibniz Institute for Solid State and Materials Research Dresden (IFW), PO Box 270116, 01171 Dresden, Germany

^{a)}Corresponding authors: emre.erdem@sabanciuniv.edu, msomer@ku.edu.tr

ABSTRACT

Nano sized magnesium diboride (MgB₂) samples were synthesized using various high-quality nano-B precursor powders. The microscopic defect structures of MgB₂ samples were systematically investigated using X-ray powder diffraction, Raman, resistivity measurements and electron paramagnetic resonance spectroscopy. A significant deviation in the critical temperature T_c was observed due to defects and crystal distortion. The symmetry effect of the latter is also reflected on the vibrational modes in the Raman spectra. Scanning electron microscopy analysis demonstrate uniform and ultrafine morphology for the modified MgB₂. Defect center in particular Mg vacancies influence the connectivity and the conductivity properties which are crucial for the superconductivity applications.

© 2019 Author(s). All article content, except where otherwise noted, is licensed under a Creative Commons Attribution (CC BY) license (<http://creativecommons.org/licenses/by/4.0/>). <https://doi.org/10.1063/1.5089488>

INTRODUCTION

Extended studies have been performed on improvement of the synthesis process of magnesium diboride (MgB₂) since its discovery in 2001.¹ The present study investigates the choice of boron precursors which is of prime importance for the functionality of MgB₂ materials and which in turn is governed by the particle size. Actually, there is a linear size correlation between the particles of the reactant boron powders and the final product MgB₂.² This means that a significant average particle size reduction for MgB₂ can be obtained only by using boron particles of submicron or nano size. The most commonly used precursor boron powders are commercially available, with the purity grades of 86-88%-wt (B-86), 90-92%-wt (B-90) and 95-97%-wt. (B-95), respectively. The powders are produced via Moissan process followed by a purification step

after which the level of the purity can be increased to a maximum of 97%-wt.³⁻⁵ The so obtained materials are semi-crystalline with a particle size range of ca. 0.8-1.2 μm .⁶ Extended studies in the last decade have revealed that the crucial factor for fabricating high performance MgB₂ powders is not the purity grade of the precursor boron but its amorphousness and the particle size, allowing a fast reaction at moderate temperatures.⁶⁻⁸ Until now, these criteria are best met by the commercially available nano-size boron powder (nano-B, Pavezyum Kimya) which is accessible via “on demand” production and “*in situ*” pyrolysis of diborane gas.^{6,9} The product is fully amorphous, exhibiting a particle size within the range of 50 to 300 nm and a purity grade of >98.5%-wt.^{6,10} One reason for the efficiency of this material is that MgB₂ powders synthesized from nano-B can be also in nano-size, wires and bulks depending on the synthesis technique. This leads to a better grain connectivity and

enhancement of J_c .¹¹⁻¹³ Furthermore, the comparatively poor crystallinity of the so-prepared powders cause structural point defects which in turn act as pinning centers improving the superconducting performance as it was reported in literature.^{2,14,15} Despite its superior features, nano-B is due to the high processing costs still about 8-10 times more expensive than the other commercial powders obtained from magnesiothermic reaction based Moissan process.¹⁶ In the last two years we have been focused on new synthesis methods and routes to improve the chemical and morphological properties of the commercial semi-crystalline B-86/-90/-95 series with the target of obtaining a cost-effective powder, revealing similar features as nano-B. Very recently, utilizing different inorganic salt mixtures in various ratios as flux, we were able to synthesize two different modified powders M-B-86 and M-B-95 which show superior properties to the commercial B-86 and B-95 regarding the amorphousness, particle size and surface activity (BET), as well as defects and chemical reactivity.¹⁷ It is worthy to note that there are alternative techniques to obtain pure boron powder effectively: via-gas and magnesiothermic reaction (mentioned above). Via-gas technique uses the hydrogen gas to reduce gaseous boron trichloride (BCl_3), whereas magnesiothermic reaction uses a combination of heat and magnesium to reduce the boron trioxide (B_2O_3) to elemental B. Such techniques revealed not only complete removal of MgO from Mg-reduced boron providing clean sources of B but also T_c of 39 K.¹⁸⁻²⁰

To test modified M-B-86 and M-B-95 powders suitability as precursor, MgB_2 samples were synthesized and characterized by means of powder x-ray diffraction (PXRD), scanning electron microscopy (SEM), transport measurements, Raman and EPR spectroscopy. In the following, we will discuss and comment on the results in context with the previously reported data for MgB_2 specimen prepared from the unmodified commercial powders B-86 and B-95.^{2,10,21}

EXPERIMENTAL

Synthesis

The two different boron powders M-B-86 and M-B-95 were prepared to modify the magnesiothermal self-propagating high temperature synthesis (SHS) process by addition of a suitable salt mixture ($\text{NaCl}/\text{CaCl}_2$; 30%-wt) which acted as a flux. The major advantage of this step is the reduction of the reaction temperature and the particle size.



The product obtained after the reaction contains beside the primary phase B and the flux, MgO and magnesium borates as major impurities. The removal of the byproducts and the salt mixture was performed by hot HCl leaching, followed by filtration, washing and drying. The purity of the boron powder at this stage is 85.9%-wt (M-B-86), comprising 10-12%-wt Mg, as well as small amounts of boron oxide and sub-oxides as further impurities. Further purification of the powder can be achieved by reduction of the Mg content. For this purpose the treatment with elemental chlorine was employed³ which yielded a powder with a purity level of 94.8%-wt (M-B-95). Modified MgB_2 samples (M- MgB_2) were prepared by using solid state synthesis techniques. Mg (99.8%) and M-B-86/M-B-95 boron

powders (molar ratio 1:2; typical batch: 2g) were grinded and placed in a steel crucible. The crucible with the reactants was then transferred into a silica tube for protection against oxidation and heated under Ar flow to 800 °C (M-B-95) and 850 °C (M-B-86), respectively. After annealing for 4 h the samples were cooled down to room temperature within 6 h.

Characterization methods

All samples were analyzed by powder x-ray diffraction (PXRD). PXRDs were recorded with a BRUKER D2 Phaser diffractometer (CuK_{α} radiation with LYNXEYETM detector). SEM images of powders were taken with Zeiss Ultra Plus FE-SEM at 2 kV accelerating voltage. CIF files for Raman analysis were done using nearly 5mg of sample in sealed Pyrex tube ($\varnothing=4\text{mm}$) in the range of 200-1400 cm^{-1} with a BURKER RFS 100/S spectrometer (Nd:YAG-Laser, 1064 nm, 200 mW). Transport measurements of the pressed samples were carried out with the four-point method in a physical property measurement system (PPMS) at external magnetic fields up to 9 T. The critical temperature T_c was determined in the heating-up resistance curve at 90% of the normal-state resistance at 40 K. The samples were specially treated for electrical measurements as follows: From powders, disk-shaped bulk samples (\varnothing 10mm, height \approx 1.5) were obtained in a vacuum chamber by hot-pressing under Ar atmosphere (500 mbar) applying a pressure of 640 MPa at 700 °C during 10 min. X-band (9.86 GHz) continuous-wave-EPR measurements were performed with a Bruker EMX spectrometer. We have used a rectangular TE102 (X-band) resonator from Bruker. The offset in the magnetic field and the exact g -factors in X-band measurements were determined with a polycrystalline DPPH (2-diphenyl-1-picrylhydrazyl) reference sample with well-known g -factor ($g=2.0036$). For cooling (to liquid helium temperatures) an Oxford CF-935 cryostat was used. The temperature was regulated by a temperature controller (Oxford ITC-503). The EPR spectral analysis has been performed using the WINEPR program from Bruker.

RESULTS AND DISCUSSION

Fig. 1 shows the PXRD patterns of M-B-86 and M-B-95 together with their primary B-86 and B-95. In both modified boron powder crystallinity has deteriorated sharply. M-B-86 shows almost amorphous powder diagram while in M-B-95 extremely low degree of crystallinity is detectable. Low crystallinity might be related to higher amorphous content of the particles which is proved by dynamic light scattering (DLS) analysis.

DLS analysis revealed that for M-B-86 particle size are <500 nm while particle size in as-received B-86 are <1400 nm. Same is valid for M-B-85 particle size which are <400 nm whereas in as-received B-95 particle size are <1000 nm. Worth mentioning are the results of the BET measurements which show a 6-8 fold increase of the surface activity for the modified powders ($\text{BET}(\text{gm}^{-2})$); B-86: 5, M-B-86: 43, B-95: 10, M-B-95: 68).

Fig. 2(a) shows the PXRD results of MgB_2 produced by B-86 (MgB_2 -86) and M-B-86 (M- MgB_2 -86) whereas Fig. 2(b) shows MgB_2 PXRD patterns which are produced by B-95 (MgB_2 -95) and M-B-95 (M- MgB_2 -95), respectively. All samples contain a trace of MgO which is originating from starting materials. Origin of MgO has been discussed previously in detail.^{2,21,22} Common phases such

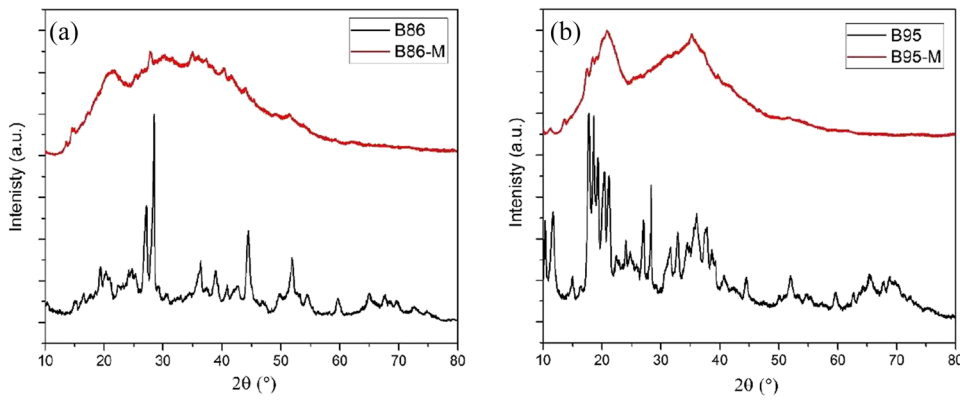


FIG. 1. PXRD patterns of (a) B-86 and M-B-86, (b) B-95 and M-B-95.

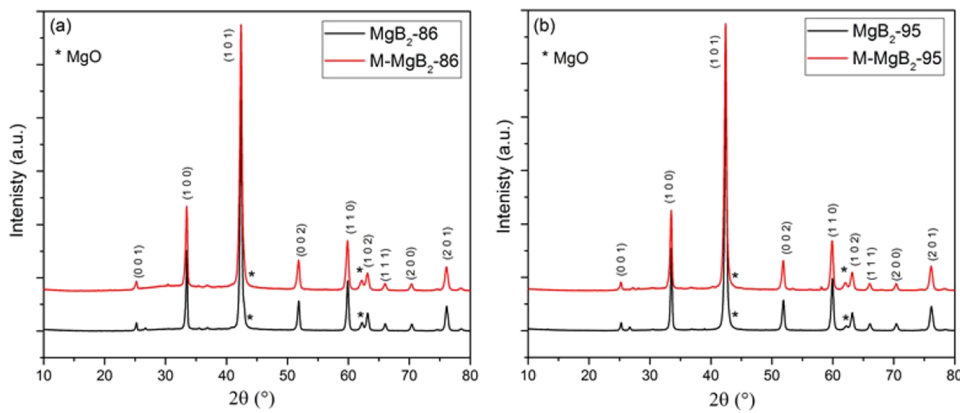


FIG. 2. PXRD patterns of (a) MgB_2 -86 and M- MgB_2 -86 (b) MgB_2 -95 and M- MgB_2 -95.

as Mg deficient borides (MgB_4 , MgB_{12} etc.) or Mg excess were not observed. By using well-known Scherrer equation and based on full-width-half-maximum (FWHM) of the peak (101), crystalline size for MgB_2 -86 and M- MgB_2 -86 are 36 and 40 nm respectively. Crystalline

size for M- MgB_2 -95 also reduced to 30 nm from 50 in MgB_2 -95. Such decrease in crystalline size in the modified MgB_2 samples is also confirmed in SEM pictures Fig. 3(b) and (d) which show the reduction the particle size.

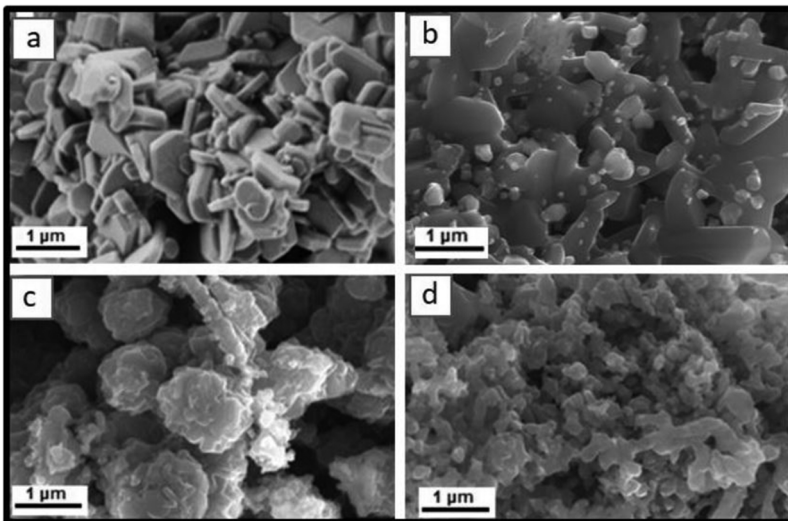


FIG. 3. SEM images of (a) MgB_2 -86, (b) M- MgB_2 -86, (c) MgB_2 -95, (d) M- MgB_2 -95.

Fig. 3(a–d) is showing the SEM images of MgB_2 -86, M- MgB_2 -86, MgB_2 -95 and M- MgB_2 -95. As shown in Fig. 3(a) and 3(c) the MgB_2 synthesized from B-86 and B-95 are prismatic and well-shaped hexagonal crystals. In contrast, M- MgB_2 -86 and M- MgB_2 -95 are formed flat shaped particles with poor crystallinity which can be well distinguished in Fig. 3(b) and 3(d). Poor crystallinity might be related to higher amorphous content of the particles with a mean size of 50–250 nm. Furthermore, the Fig. 3(b) and (d) reveals that the particles of the M- MgB_2 -86 and M- MgB_2 -95 are more uniform and smaller compared to those of MgB_2 -86, MgB_2 -95 in Fig. 3(a) and 3(c). The reason of the particle sizes difference in these MgB_2 samples might be related to particle size of the starting B powders.²² In M-B-86 and M-B-95 particles size are smaller than B-86 and B-95 which yield smaller size MgB_2 particles. Present results are in line with those reported in following Refs. 22–24, highlighting the direct role of starting B particle size in the size of synthesized MgB_2 .

Resistivity as a function of temperature for pressed M- MgB_2 -86, MgB_2 -95 and M- MgB_2 -95 are depicted in Fig. 4. Based on the resistivity curve, T_c is increasing from M- MgB_2 -95 (lowest T_c) to M- MgB_2 -86 (highest T_c). T_c increment from M- MgB_2 -95 to M- MgB_2 -86 can be explained by higher annealing temperature and better crystallinity of MgB_2 particles in M- MgB_2 -86 rather than M- MgB_2 -95 which can be also seen in SEM images.²⁵ Moreover, the shape of resistivity curve for all samples at temperature higher than 37 K (above the superconducting transition) exhibit a metallic behavior.^{26–28} However that maximum resistivity at room temperature ρ_{300} (metallic resistivity) in M- MgB_2 -86 is more than ρ_{300} in of M- MgB_2 -95 and MgB_2 -86 samples. ρ_{300} for M- MgB_2 -95 is 28.0 $\mu\Omega\text{cm}$ while for MgB_2 -95 and for M- MgB_2 -86 are 31.1 $\mu\Omega\text{cm}$ and 36.4 $\mu\Omega\text{cm}$, respectively.

Resistivity in MgB_2 will be effected by electron scattering due to defects, impurities and phonons.^{29–31} All will be caused in increment in electron scattering and reduce their mobility. Therefore higher resistivity in M- MgB_2 -86 might originate from lower purity in M-B-86 which is used to synthesize this compound.

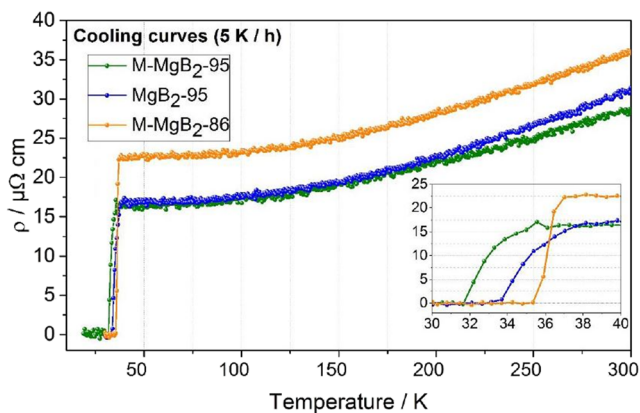


FIG. 4. Variation of temperature dependence of resistivity for MgB_2 -95, M- MgB_2 -95 and M- MgB_2 -86 samples at 0 T. The obtained resistivity values are as follows at 300 K: ρ_{300} 31.1 $\mu\Omega\text{cm}$ for MgB_2 -95, 28.0 $\mu\Omega\text{cm}$ for M- MgB_2 -95 and 36.4 $\mu\Omega\text{cm}$ for M- MgB_2 -86.

TABLE I. The values of measured resistivity (ρ), residual resistivity ratio (RRR) and active cross-sectional area fractions (AF) for MgB_2 -95, M- MgB_2 -95 and M- MgB_2 -86 samples.

Sample	ρ 40 $\mu\Omega\text{cm}$	ρ 300 $\mu\Omega\text{cm}$	$\Delta\rho$ (ρ 300- ρ 40) $\mu\Omega\text{cm}$	RRR	AF
MgB_2 -95	17.6	31.1	13.5	1.767	0.541
M- MgB_2 -95	15.9	28.0	12.1	1.761	0.603
M- MgB_2 -86	22.5	36.4	13.9	1.618	0.525

Table I summarizes connectivity information according to Fig. 4 for MgB_2 -95, M- MgB_2 -95 and M- MgB_2 -86 samples. Based on Rowell connectivity analysis, AF value (the active cross-sectional area fraction) shows the quality of connectivity between the grains.^{28,32,33} The enhanced connectivity in M- MgB_2 -95 originates from the reduced grain size in comparison to other samples. Low AF factor in M- MgB_2 -86 in comparison to other MgB_2 -95 and M- MgB_2 -95 would be also related to purity and grain size effect in this material.

Since MgB_2 is a phonon-mediated superconductor, electron-phonon interaction plays an important role in the pairing mechanism that is responsible for MgB_2 superconductivity. Therefore it is important to apply Raman spectroscopy to understand the Raman active vibration modes, thus defect structures. It is well known that for the P_{6mm} space group to which MgB_2 belongs, only the E_{2g} in-plane B stretching mode is Raman active. This mode is highly depending on the morphology, sample size, temperature and the defect structures. Here in Fig. 5, E_{2g} appeared at 591 cm^{-1} with anomalously large Lorentzian linewidth for all samples. Since E_{2g} is the only and dominant Raman mode we do not see much difference between the samples. This is closely related to the detection limit of Raman spectroscopy where we cannot get further information about the anharmonicity. Such phonon anomaly including anharmonicity and multi-phonon contributions can be closely relate with the point defects. Further elaborate this approach EPR spectroscopy is one of the important techniques for understanding defect structures since EPR has extensively sensitive and high detection limit for paramagnetic defects.

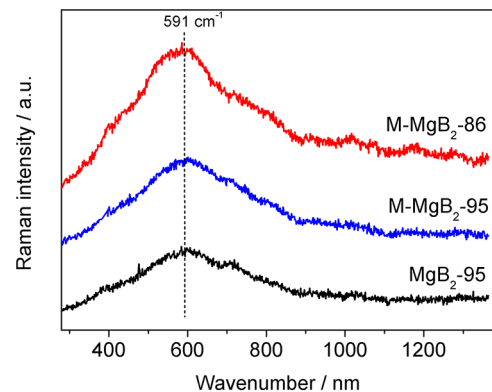


FIG. 5. Raman spectroscopy measurements for MgB_2 synthesized from MgB_2 -95, M- MgB_2 -95 and M- MgB_2 -86.

EPR does not only work very well on the detection of paramagnetically active point defects but also one may obtain reliable correlation to the electronic and structural properties of MgB_2 . Up to now, very limited studies have been reported for investigating the defect structures of MgB_2 by the aid of EPR.^{34,35} Spectral changes in EPR signal mostly attributed to the changes in local crystalline field symmetry around weakly localized conduction electrons or holes. Conceivably possible defect centers in MgB_2 could be the Mg vacancies (V_{Mg}), oxygen vacancies (V_{O}), boron vacancies (V_{B}) and the interstitials (O_i or B_i). In particular effect of Mg vacancy in MgB_2 on structural and superconducting properties has been discussed controversially.³⁶⁻³⁸ Although controversy exists, in those works together with the reduction in T_c and coexistence of superconductive and non-superconductive electronic phases has been correlated with the poor and rich regions of Mg vacancies. There are two main sources for oxygen related defect centers: oxygen vacancies may be formed in the minor boron oxide or magnesium oxide phases, persistent in both the amorphous B powder and the grain boundaries of the MgB_2 samples.³⁸ In this study highest grade B powders were used that's why the only source for V_{O} is the formation of MgO secondary phase which is also observed in PXRD in Fig. 2. In Fig. 6 we present the temperature dependent EPR data of three MgB_2 samples. Here we present the most interesting temperature region (30-60 K) for MgB_2 material. At paramagnetic defect state (normal state), according to their g -factors (close to free-electron g -factor: 2.0023) such defect signals can be attributed to V_{O} either on the grain boundaries or on the surface of MgB_2 since MgO is present as a secondary phases. By reducing the temperature down

to T_c (~ 39 K) both paramagnetic defect states and non-resonant superconductive states coexist. This feature occurs slightly at different temperatures from sample to sample. But it is common feature for all samples. Below a certain temperature normal states does not exist anymore and the EPR spectra ends up with the huge superconductive state where defect signal smears out and at $g \sim 2$ region only cavity/resonator signal left with very low signal-to-noise. Here it is worth to note that, as it is depicted in resistivity measurements the metallic character of the samples has been observed in EPR measurements as well. This can be understood from the typical Dysonian^{2,39} lineshape of EPR lines indicating more metallic character, thus high concentration of conduction electrons. Such conduction electrons play crucial role in the superconductive properties of MgB_2 material. For instance, the upper critical field decreases with increase of defects density and there is a strong coupling between the conduction electrons and the Raman active E_{2g} phonon, in which neighboring boron atoms move in opposite directions within the plane. When we compare each sample M-MgB₂-95 is quite interestingly shows highest T_c where superconducting and paramagnetic states both exist at 35 K. In other two samples superconductive state starts at lower temperatures 34.5 and 33.5 K for M-MgB₂-86 and MgB₂-95, respectively. Furthermore, spin counting procedure were applied where one can quantitatively determine the absolute concentration of defect centers, in other words, unpaired electrons. By the aid of, thanks to EPR, it is possible to determine the concentration of EPR at 60 and 34.5 K which are listed in Table II.

Here it is important to note that previously we investigated Al doped MgB_2 by Raman and EPR spectroscopy to check the effect of

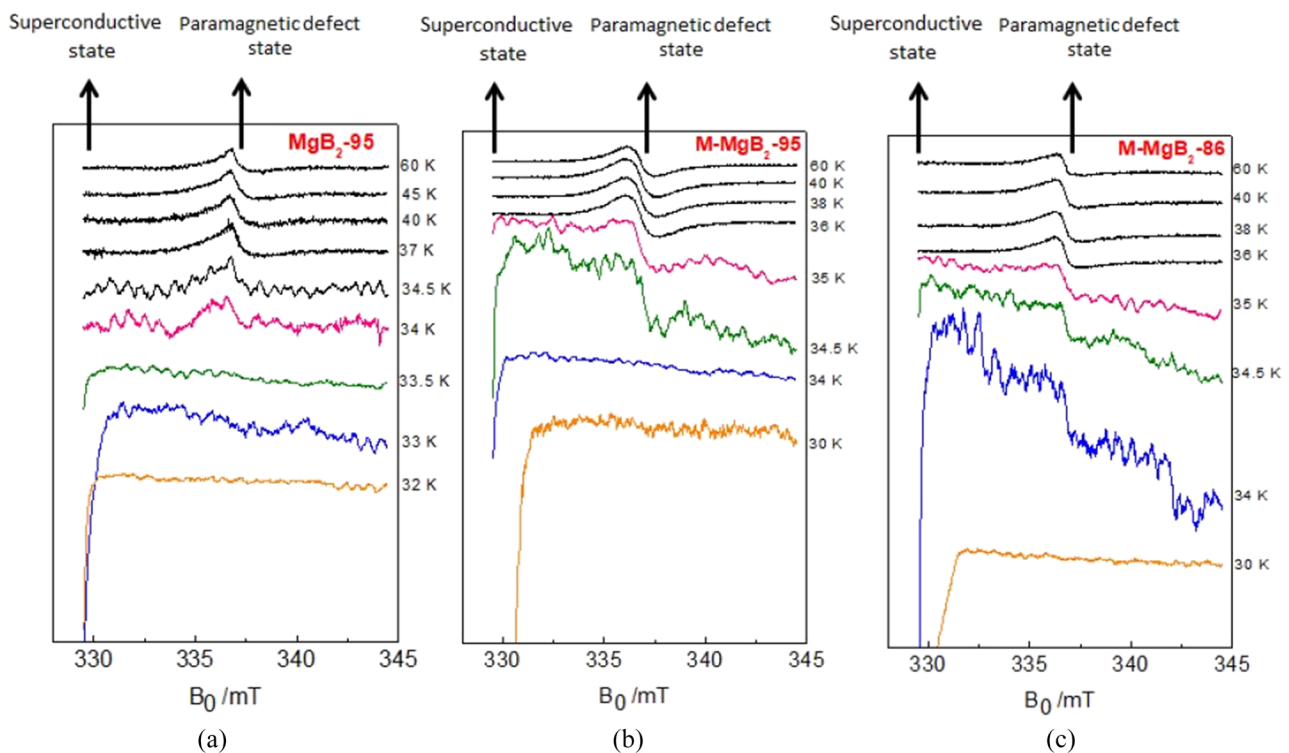


FIG. 6. Low-temperature EPR measurements for MgB_2 synthesized from (a) MgB_2 -95, (b) M-MgB₂-95 and (c) M-MgB₂-86.

TABLE II. Defect concentrations obtained from spin counting procedure. Details of spin counting can be found in the electronic supplementary material.

	Defect concentration at 60 K	Defect concentration at 34.5 K	Defect concentration below 34 K
MgB ₂ -95	6.4x10 ¹⁴ spins/mg	1.7x10 ¹¹ spins/mg	0
M-MgB ₂ -95	2.2x10 ¹⁵ spins/mg	3.7x10 ¹² spins/mg	0
M-MgB ₂ -86	8.3x10 ¹⁴ spins/mg	4.5x10 ¹¹ spins/mg	0

Mg vacancies. EPR results were in agreement with the findings in Raman spectra which prove that the paramagnetically active structural defects are mainly related to the Mg-vacancies. Combined Raman and EPR results are clearly demonstrated that the effects of structural defects on the electronic properties are gradually quenched by increasing Al or decreasing Mg contents. This confirms that the paramagnetism of MgB₂ at room temperature is strongly related to V_{Mg}. And such V_{Mg} are coexisting with V_O defects in the MgB₂ samples where V_O are always there at a certain amount (for free) due to MgO impurities. Further one may now address the effect of extra pinning centers due to defects.

EPR results is presented here give further understanding of the competing effects between defect states at the temperatures below and above superconducting states MgB₂. It is clearly visible that below critical temperature the superconducting phase become dominant and the defect centers quenched. This shows that above T_c the defect centers play crucial role for critical temperature thus critical current density J_c.

CONCLUSIONS

The results in this work showed the importance of defect structures in MgB₂ and their roles and effects on the superconductive properties. The quality of starting materials in particular B powder precursors are highly important to control the defects thus the superconductivity and size. Here we have selected three different sample systems with different grades and they all showed not only different electronic properties such as defect distributions in MgB₂ nanocrystal lattice but also significant changes in T_c and resistivity values. Nowadays to have high technological application of MgB₂ materials for instance nanowires for high energy applications it is necessary to produce well defined MgB₂ products with high quality. From this point of view present work may serve superconductive research and development engineers in a sense that intrinsic defects should be controlled for high performance and extensive functionality.

SUPPLEMENTARY MATERIAL

See [supplementary material](#) for detailed description of spin counting procedure.

ACKNOWLEDGMENTS

We thank Baris Yagcioglu and Kamil Kiraz for their support to collect SEM data.

REFERENCES

- J. Nagamatsu, N. Nakagawa, T. Muranaka, Y. Zenitani, and J. Akimitsu, "Superconductivity at 39 K in magnesium diboride," *Nature* **410**, 63–64 (2001).
- A. Bateni, S. Repp, R. Thomann, S. Acar, E. Erdem, and M. Somer, "Defect structure of ultrafine MgB₂ nanoparticles," *Appl. Phys. Lett.* **105**, 202605 (2014).
- A. Kozyrev, "Effect of temperature and pressure to pinning centers in bulk MgB₂ under high pressure," *Low Temperature Physics* **40**, 752 (2014).
- J. Akimitsu, S. Akutagawa, K. Kawashima, and T. Muranaka, "Superconductivity in MgB₂ and its related materials," *Progress of Theoretical Physics Supplement* **159**, 326 (2005).
- J. A. Kohn, W. F. Nye, and G. K. Gaulé, eds., *Boron Synthesis, Structure, and Properties. Proceedings of the Conference on Boron*, Springer US, Boston, MA, 1960.
- R. Flükiger and R. Flükiger, eds., *MgB₂ superconducting wires. Basics and applications*, World Scientific Publishing Co. Pte Ltd, Vol. 2, Singapore, 2016.
- X. Xu, D. I. dos Santos, J. H. Kim, W. K. Yeoh, M. J. Qin, K. Konstantinov, and S. X. Dou, "Effect of boron powder purity on superconducting properties of bulk MgB₂," *Physica C: Superconductivity and its Applications* **460–462**, 602–603 (2007).
- T. Matsushita, M. Kiuchi, A. Yamamoto, J. Shimoyama, and K. Kishio, "Critical current density and flux pinning in superconducting MgB₂," *Physica C: Superconductivity* **468**, 1833–1835 (2008).
- S. Acar, Koc University, PhD thesis, 2012.
- Ö. Balci, S. Acar, M. Rafieezad, and M. Somer, Review on magnesium diboride (MgB₂) as excellent superconductor: Effects of the production techniques on the superconducting properties, *Bor Dergisi*, **2**.
- K. Matsuzaki, K. Hanada, K. Hatsukano, T. Shimizu, S. Suzuki, and S. Fuchizawa, "Effect of boron particle size on the formation and superconductivity of MgB₂," *J. Jpn. Soc. Powder Powder Metallurgy* **50**, 306–309 (2003).
- J.-H. Ahn and S. Oh, "Pore structures and grain connectivity of bulk MgB₂," *Physica C: Superconductivity* **469**, 1235–1238 (2009).
- S. Barua, D. Patel, N. Alzayed, M. Shahabuddin, J. M. Parakkandy, M. S. Shah, Z. Ma, M. Mustapić, M. S. Al Hossain, and J. H. Kim, "Correlation between in-field J_c enhancement and grain connectivity in co-doped MgB₂ superconductor," *Materials Letters* **139**, 333–335 (2015).
- Y. Zhu, A. V. Pogrebnjakov, R. H. Wilke, K. Chen, X. X. Xi, J. M. Redwing, C. G. Zhuang, Q. R. Feng, Z. Z. Gan, R. K. Singh, Y. Shen, N. Newman, J. M. Rowell, F. Hunte, J. Jaroszynski, D. C. Larbalestier, S. A. Baily, F. F. Balakirev, and P. M. Voyles, "Nanoscale disorder in pure and doped MgB₂ thin films," *Superconductor Science and Technology* **23**, 095008 (2010).
- Y. Zhu, D. C. Larbalestier, P. M. Voyles, A. V. Pogrebnjakov, X. X. Xi, and J. M. Redwing, "Nanoscale disorder in high critical field, carbon-doped MgB₂ hybrid physical-chemical vapor deposition thin films," *Appl. Phys. Lett.* **91**, 082513 (2007).
- M. Vignolo, G. Bovone, C. Bernini, A. Palenzona, S. Kawale, G. Romano, and A. S. Siri, "High temperature heat treatment on boron precursor and PIT process optimization to improve the J_c performance of MgB₂-based conductors," *Supercond. Sci. Technol.* **26**, 105022 (2013).
- M. Somer, A. Bateni, and S. Acar, eds., *Novel Boron-86 and Boron-95 Powders with superior Properties: Synthesis and Characterization*, 2016.

- ¹⁸M. Vignolo, G. Romano, A. Martinelli, C. Bernini, and A. S. Siri, "A novel process to produce amorphous nanosized boron useful for MgB₂ synthesis," *IEEE Trans. Appl. Supercond.* **22**, 6200606 (2012).
- ¹⁹J. V. Marzik, R. C. Lewis, M. R. Nickles, D. K. Finnemore, J. Yue, M. Tomsic, M. Rindfleisch, and M. D. Sumption, "Plasma synthesized boron nano-sized powder for MgB₂ wires," *AIP Conference Proceedings* **1219**, 295 (2010).
- ²⁰A. F. Zhigach and D. C. Stasinevich, in *Boron and Refractory Borides*, ed. V. I. Matkovich, Springer Berlin Heidelberg, Berlin, Heidelberg, 1977, pp. 214–226.
- ²¹A. Bateni, E. Erdem, S. Repp, S. Acar, I. Kokal, W. Häföler, S. Weber, and M. Somer, "Electron paramagnetic resonance and Raman spectroscopy studies on carbon-doped MgB₂ superconductor nanomaterials," *Journal of Applied Physics* **117**, 153905 (2015).
- ²²A. Bateni, E. Erdem, S. Repp, S. Weber, and M. Somer, "Al-doped MgB₂ materials studied using electron paramagnetic resonance and Raman spectroscopy," *Appl. Phys. Lett.* **108**, 202601 (2016).
- ²³S. K. Chen, K. A. Yates, M. G. Blamire, and J. L. MacManus-Driscoll, "Strong influence of boron precursor powder on the critical current density of MgB₂," *Supercond. Sci. Technol.* **18**, 1473 (2005).
- ²⁴Y. Zhang, "Influence of nanocrystalline boron precursor powder on superconductivity in MgB₂ bulk," *J. Nanosci. Nanotech.* **9**, 7402 (2009).
- ²⁵Y. Feng, Y. Zhao, A. K. Pradhan, L. Zhou, P. X. Zhang, X. H. Liu, P. Ji, S. J. Du, C. F. Liu, Y. Wu, and N. Koshizuka, "Fabrication and superconducting properties of MgB₂ composite wires by the PIT method," *Supercond. Sci. Technol.* **15**, 12 (2001).
- ²⁶S. S. Indrakanti, V. F. Nesterenko, M. B. Maple, N. A. Frederick, W. H. Yuhasz, and S. Li, "Hot isostatic pressing of bulk magnesium diboride," *Philosophical Magazine Letters* **81**, 849–857 (2010).
- ²⁷L. M. León-Rossano, "An inexpensive and easy experiment to measure the electrical resistance of high-T_c superconductors as a function of temperature," *American Journal of Physics* **65**, 1024–1026 (1997).
- ²⁸J. M. Rowell, "The widely variable resistivity of MgB₂ samples," *Supercond. Sci. Technol.* **16**, R17 (2003).
- ²⁹B. Gahtori, R. Lal, S. K. Agarwal, Y. K. Kuo, K. M. Sivakumar, J. K. Hsu, J. Y. Lin, A. Rao, S. K. Chen, and J. L. MacManus-Driscoll, "Effects of Fe substitution on the transport properties of the superconductor MgB₂," *Phys. Rev. B* **75**, 684 (2007).
- ³⁰R. Prozorov, M. Kończykowski, M. A. Tanatar, A. Thaler, S. L. Bud'ko, P. C. Canfield, V. Mishra, and P. J. Hirschfeld, "Effect of electron irradiation on superconductivity in single crystals of Ba(Fe_{1-x}Ru_x)₂As₂ (x=0.24)," *Phys. Rev. X* **4**, 1781 (2014).
- ³¹A. Vajpayee, R. Jha, A. K. Srivastava, H. Kishan, M. Tropeano, C. Ferdeghini, and V. P. S. Awana, "The effect of synthesis temperature on the superconducting properties of n-SiC added bulk MgB₂ superconductor," *Supercond. Sci. Technol.* **24**, 045013 (2011).
- ³²J. Jiang, B. J. Senkowicz, D. C. Larbalestier, and E. E. Hellstrom, "Influence of boron powder purification on the connectivity of bulk MgB₂," *Supercond. Sci. Technol.* **19**, L33 (2006).
- ³³X. Xu, J. H. Kim, S. X. Dou, S. Choi, J. H. Lee, H. W. Park, M. Rindfleisch, and M. Tomsic, "A correlation between transport current density and grain connectivity in MgB₂/Fe wire made from ball-milled boron," *J. Appl. Phys.* **105**, 103913 (2009).
- ³⁴M. K. Bhide, R. M. Kadam, M. D. Sastry, A. Singh, S. Sen, D. K. Aswal, S. K. Gupta, and V. C. Sahni, "Magnetic field dependent microwave absorption studies on a MgB₂ superconductor," *Supercond. Sci. Technol.* **14**, 572 (2001).
- ³⁵Y. Köseoglu, B. Aktaş, F. Yildiz, D. K. Kim, M. Toprak, and M. Muhammed, "ESR studies on high-T_c superconductor MgB₂," *Physica C: Superconductivity* **390**, 197–203 (2003).
- ³⁶Y. Zhong, H. Zhu, L. L. Shaw, and R. Ramprasad, "Ab initio computational studies of Mg vacancy diffusion in doped MgB₂ aimed at hydriding kinetics enhancement of the LiBH₄ + MgH₂ system," *J. Phys. Chem. C* **114**, 21801–21807 (2010).
- ³⁷N. D. Zhigadlo, S. Katrych, J. Karpinski, B. Batlogg, F. Bernardini, S. Massidda, and R. Puzniak, "Influence of Mg deficiency on crystal structure and superconducting properties in MgB₂ single crystals," *Phys. Rev. B* **81**, 159 (2010).
- ³⁸V. Likodimos and M. Pissas, "Electron spin resonance and microwave absorption study of MgB₂," *Phys. Rev. B* **65**, 63–39 (2002).
- ³⁹A. H. El-Sayed, G. J. Nieuwenhuys, J. A. Mydosh, and K. H. J. Buschow, "Electron spin resonance in ternary intermetallic compounds with MgAgAs structure," *J. Phys. F: Met. Phys.* **18**, 2265.